Chaos, Solitons and Fractals 166 (2023) 112887

Contents lists available at ScienceDirect

Chaos, Solitons and Fractals

journal homepage: www.elsevier.com/locate/chaos

# Optimal added noise for minimizing distortion in quantizer-array linear estimation

Tianting Xie [a,*], Yuandong Ji [b], Zhongshan Yang [a], Fabing Duan [c], Derek Abbott [d]

[a] School of Statistics, Dongbei University of Finance and Economics, Dalian 116025, PR China
[b] School of Aeronautics and Astronautics, Sichuan University, Chengdu 610065, PR China
[c] Institute of Complexity Science, Qingdao University, Qingdao 266071, PR China
[d] Centre for Biomedical Engineering (CBME) and School of Electrical and Electronic Engineering, The University of Adelaide, South Australia 5005, Australia

ARTICLE INFO

*Keywords:*
Suprathreshold stochastic resonance
Optimal added noise
Quantizer-array
Signal estimation
Distortion

ABSTRACT

For linearly estimating the input signal, the optimization of suprathreshold stochastic resonance in an array of $N$ parallel $M$-ary quantizers is theoretically investigated. We first prove that the mean square error (MSE) of the designed quantizer-array is a convex functional with respect to the cumulative probability function (CDF) of the added noise. Then, for an arbitrary input signal and the quantization interval being $N$ times the decoding step size, we theoretically demonstrate that minimum MSE distortion can be obtained for optimal added uniform noise. Furthermore, for a uniform input signal, the optimality condition also holds if the system parameters and the boundary of the signal satisfy an inequality constraint condition. Moreover, under this condition, the optimal parameters of the quantizer-array can be also determined exactly. By applying both the optimal added noise and optimal parameters to the quantizer-array, the MSE can be further improved for larger array size $N$ or quantization order $M$. Finally, the optimal added noise is also discussed for minimizing distortions of the quantizer-array linear estimation in the presence of the background noise.

## 1. Introduction

Noise is ubiquitous especially in complex systems. In general, it arises from environmental perturbations, the natural random variation of the system parameters, or internal thermal fluctuations [1]. Noise used to be thought detrimental in any circumstance, but the fact is that it can play a constructive role [2–5]. For instance, the presence of noise may increase the degree of order rather than disorder [1], which turns out to be beneficial. Intentionally added noise to the inputs of convolutional neural networks (CNNs) has been shown to enhance deep learning [6]. The response to noise can even shape the behavior of systems. Cavagna et al. discovered that animal groups such as bird flocks work in a self-organized way so as to acquire a better global response to environmental perturbations under the pressure of predation [7]. The main proponent, Parisi, was awarded the 2021 Nobel Prize in Physics for his contributions to "the discovery of the interplay of disorder and fluctuations in physical systems from atomic to planetary scales" [8].

In certain nonlinear dynamic systems, noise can assist weak signals in crossing the potential barrier, thereby improving the performance of these systems. This effect was first introduced by Benzi et al. under the name "stochastic resonance" (SR) [2]. Besides, noise can also be beneficial for inducing phase transitions [9–14] or enhancing the stability of metastable states [15–17]. Such noise-induced effects have also been referred to as noise-enhanced [18–20], noise-aided effects [21,22], or stochastic facilitation [4,23] in subsequent studies. To date, noise-induced effects have been observed in a wide variety of natural or artificial systems in physics [24–26], biology [19,27,28], ecology [29,30], engineering [31–33], etc. The type of noise is usually assumed to be Gaussian due to its convenient statistical properties [34–36]. However, non-Gaussian noise has been observed in numerous systems [25,37,38]. For those types of noise exhibiting abrupt jumps and rapid variations, an $\alpha$-stable Lévy distribution provides a better description [12,28,39]. The exploration of the constructive role of non-Gaussian noise is also very interesting in many practical situations.

In the early days of SR research, the signal was required to be below the potential barrier or the crossing threshold of the system [36,40–43]. Notwithstanding, Stocks discovered that, in multilevel threshold systems, the noise-enhanced effects can be extended to the case of suprathreshold signal strengths [44,45], this is the suprathreshold SR (SSR). Accordingly, this effect in multilevel threshold systems has received considerable attention due to potential applications in analog-to-digital converters [31,35,46], cochlear implants [34,47], signal detection and estimation [37,48,49], neural modeling [35,50–55],

* Corresponding author.
*E-mail address:* xietianting@dufe.edu.cn (T. Xie).

https://doi.org/10.1016/j.chaos.2022.112887
Received 14 September 2022; Received in revised form 28 October 2022; Accepted 7 November 2022
Available online 22 November 2022

neural networks [56–58], and so on. The performance measurements of the SSR effect involve mutual information [59–61], output signal-to-noise ratio (SNR) [23,62], signal-to-quantization-noise ratio [63–65], Fisher information [23,66], input–output cross correlation [37,67], mean square error (MSE) [68–70], etc.

The SSR effect has been extensively discussed in multilevel threshold systems consisting of parallel binary quantizers [19,32,44,45]. A large number of discussions concern the optimal system parameters for a given added noise type. If all the binary quantizers are identical, the transmitted information evaluated by the mutual information is maximized when all thresholds are set to coincide with the signal mean [45]. Otherwise, if the thresholds in different binary quantizers vary independently, the optimal threshold distributions depend on the input SNR [62,71]. For signal estimation or reconstruction, a decoder is usually connected to a multilevel threshold system. In terms of linear decoding criteria, the decoding step size that minimizes the MSE depends on both the signal and the multilevel threshold system according to Wiener optimal linear decoding [32]. Furthermore, the output of each quantizer is endowed with a weight coefficient, and the optimally weighted quantizer array is proven to provide a lower MSE in comparison with the unweighted array [72,73].

Since the addition of noise can be arbitrarily designed to improve the system performance within the framework of SR, then finding the optimal type of added noise becomes an interesting question [74–76]. Particularly, for an array of identical binary quantizers, optimal types of noise have been studied analytically [61,69,77]. If the input signal is discrete (binary), the optimal added noise that maximizes the mutual information is found to have a finite distribution form [61]. In contrast, for a continuous signal, the corresponding optimal added noise becomes a constant bias [61]. It is proven that uniform noise gives the fastest MSE decrease in the small-noise limit among all zero-symmetric scale-family noise types with finite variance [69]. Further, the uniform noise, among all types of added noise, is also proven to yield the lowest MSE distortion of parallel binary quantizer-arrays on signal quantization [77].

McDonnell et al. extended the binary quantizer-array to the $M$-ary situation and discussed $M$-ary SSR behaviors in terms of mutual information [35] and signal-to-quantization-noise ratio [63]. In [35], the $M$-ary quantizer-array assisted by added Gaussian noise is investigated as a case study of a stochastic pooling network. The loss in the mutual information before and after pooling by summation shows a double peak as the input SNR increases. In [63], the scaling of the optimal input SNR as well as the maximum signal-to-quantization-noise ratio was analyzed numerically for a uniformly distributed signal buried in the added Gaussian noise. Subsequently, the corresponding signal-dependent noise situation was considered [64], and the effects of three different threshold boundaries on $M$-ary SSR were compared [64]. Optimal weights and threshold distributions under the assumptions of Gaussian distributed signal and noise were discussed in [65], which indicates that the random thresholds are the optimal thresholds setting in the context of $M$-ary SSR.

However, for the $M$-ary quantizer-array, the added noise type is usually assumed aforehand and the research conclusions are only elicited on time-consuming numerical experiments. Analytical studies are needed and the optimal type of noise for $M$-ary SSR is still unknown. Therefore, in this study, we theoretically investigate the optimization of $M$-ary SSR for minimizing distortion in quantizer-array linear estimation. First, we theoretically prove the optimal added noise type under certain conditions for an arbitrary input signal. Second, we analytically derive the optimal parameters of the designed quantizer-array, including the quantization level interval and linear decoding step size, for uniform input signal buried in added optimal uniform noise. The rest of the paper is organized as follows: Section 2 describes the model and performance metric. Section 3 explores the optimal added noise in $M$-ary quantizer-array. Section 4 discusses the optimal parameters of quantizer-array for a uniform input signal. Section 5 analyzes the optimal added noise for minimizing MSE distortion in the presence of background noise. Finally, Section 6 concludes the paper.

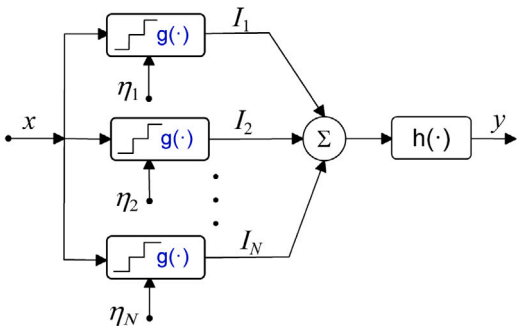


**Fig. 1.** Schematic diagram of the $M$-ary quantizer-array connected to a linear decoder $h(\cdot)$. This parallel array consists of $N$ quantizers. Each quantizer, modeled by the same quantization function $g(\cdot)$, is subject to the same signal $x$ but mutually independent added noise components $\eta_i$ with the common probability distribution. The outputs of each quantizer are $I_i \in \{0, 1, \dots, M\}$ for $i = 1, 2, \dots, N$. The summation $I = \sum_{i=1}^{M} I_i$ belongs to the set of $\{0, 1, \dots, NM\}$.

## 2. Model

### 2.1. Definitions and notation

As shown in Fig. 1, the $M$-ary quantizer-array consists of $N$ parallel quantizers $g(\cdot)$ and a linear decoder $y = h(I)$. Each quantizer is subject to the same zero-mean signal $x$ but with independently identical distributed (i.i.d.) noise components $\eta_i(t)$ for $i = 1, 2, \dots, N$. The $M$ quantization levels of each quantizer are denoted by $\{u_1, u_2, \dots, u_M\}$ and are supposed to be equally spaced. Specifically, the initial level

$$u_1 = \begin{cases} 0, & M = 1, \\ -L_u, & \text{otherwise}, \end{cases} \tag{1}$$

and $u_k = u_1 + \Delta_u(k-1)$ for $k = 2, 3, \dots, M$. Here, $L_u$ represents the positive boundary of the quantization levels. The interval $\Delta_u$ is set to $2L_u/(M-1)$ so that $\{u_1, u_2, \dots, u_M\}$ are unbiased on $[-L_u, L_u]$. Each quantizer is modeled by the quantization function

$$g(x) = k, \quad x \in [u_k, u_{k+1}) \tag{2}$$

for $k = 0, 1, \dots, M$, where $u_0 = -\infty$ and $u_{M+1} = +\infty$. Hence, the output $I_i = g(x+\eta_i)$ of the $i$th quantizer takes values from the set $\{0, 1, \dots, M\}$, and the summation $I = \sum_{i=1}^{N} I_i$ of the quantizer-array belongs to the set $\{0, 1, \dots, NM\}$. For estimating the input signal, the linear decoder in Fig. 1 is given by

$$y = h(I) = \Delta_y I - \frac{\Delta_y NM}{2} \tag{3}$$

with the decoding step size $\Delta_y$. Then, the values of $y$ are equally spaced on the interval $[-\Delta_y NM/2, \Delta_y NM/2]$.

### 2.2. MSE distortion of the designed quantizer-array

In order to measure the distortion between the input signal and the decoder, we employ the MSE calculated as [77]

$$\begin{aligned} D = \mathrm{E}\left[(y-x)^2\right] &= \int_{-\infty}^{+\infty}\int_{-\infty}^{+\infty} p_x(x)p_{y|x}(y|x)(y-x)^2\,\mathrm{d}x\mathrm{d}y \\ &= \int_{-\infty}^{+\infty} p_x(x)\left\{\sum_{k=0}^{NM} P\{I=k|x\}\,[h(k)-x]^2\right\}\mathrm{d}x \\ &= \int_{-\infty}^{+\infty} p_x(x)\left\{\Delta_y^2\mathrm{E}[I^2|x] + 2\Delta_y(y_0-x)\mathrm{E}[I|x] + (y_0-x)^2\right\}\mathrm{d}x \end{aligned} \tag{4}$$

to evaluate the estimated performance of the designed quantizer-array. Here, $p_x$ is the probability density function (PDF) of the input $x$, $p_{y|x}(y|x)$ is the conditional PDF of $y$ given $x$, and $y_0$ represents $h(0)$ for

simplicity. The conditional expectations of $I$ and $I^2$ given $x$ are denoted by $\mathrm{E}[I|x]$ and $\mathrm{E}[I^2|x]$, which can be expressed as Eqs. (A.4) and (A.5) (see Appendix A), respectively.

Substituting Eqs. (A.4) and (A.5) into Eq. (4) gives

$$\begin{aligned} D = \int_{-\infty}^{+\infty} p_x(x) \Bigg\{ & \Delta_y^2 N(N-1) \left[\sum_{k=1}^{M} F_\eta(u_k - x) - M\right]^2 \\ & + \Delta_y N \sum_{k=1}^{M} F_\eta(u_k - x)\left(\Delta_y - 2\Delta_y k - 2y_0 + 2x\right) \\ & + 2NM\Delta_y(y_0 - x) + (y_0 - x)^2 + \Delta_y^2 NM^2 \Bigg\} \mathrm{d}x, \end{aligned} \tag{5}$$

where $F_\eta$ is the cumulative density function (CDF) of the added noise and $D$ is a functional of $F_\eta$. Our main aim is to find the optimal CDF $F_\eta^{\mathrm{opt}}$ that minimizes the MSE $D$, that is:

$$F_\eta^{\mathrm{opt}} = \arg\min_{F_\eta \in \mathscr{F}} D(F_\eta), \tag{6}$$

where $\mathscr{F}$ is the set of CDFs of all random variables.

## 3. Optimal added noise for the designed quantizer-array

For any $\alpha \in [0,1]$ and $F_\eta$, $F_{\eta'} \in \mathscr{F}$, it is easy to verify that $\alpha F_\eta + (1-\alpha)F_{\eta'} \in \mathscr{F}$, indicating that $\mathscr{F}$ is a convex set. Moreover,

$$\begin{aligned} & D\left[\alpha F_\eta + (1-\alpha)F_{\eta'}\right] - \left[\alpha D(F_\eta) + (1-\alpha)D(F_{\eta'})\right] \\ & = \Delta_y^2 N(N-1) \int_{-\infty}^{+\infty} p_x(x) \Bigg\{ -\alpha \left[\sum_{k=1}^{M} F_\eta(u_k - x) - M\right]^2 \\ & \quad - (1-\alpha)\left[\sum_{k=1}^{M} F_{\eta'}(u_k - x) - M\right]^2 \\ & \quad + \left[\alpha \sum_{k=1}^{M} F_\eta(u_k - x) + (1-\alpha)\sum_{k=1}^{M} F_{\eta'}(u_k - x) - M\right]^2 \Bigg\} \mathrm{d}x \\ & = \Delta_y^2 N(N-1)\alpha(\alpha - 1) \\ & \quad \times \int_{-\infty}^{+\infty} p_x(x) \left\{ \sum_{k=1}^{M} \left[F_\eta(u_k - x) - F_{\eta'}(u_k - x)\right] \right\}^2 \mathrm{d}x \le 0. \end{aligned} \tag{7}$$

Hence, $D(F_\eta)$ is a convex functional defined on $\mathscr{F}$, and the global optimization problem in Eq. (6) can be solved with local optimization methods. For $N > 1$ and $M = 1$, the optimal noise that minimizes MSE has been proven to be uniform for any signal [77]. For $M > 1$, we prove that if either of the following conditions

(C-1) $\Delta_y = \Delta_u / N$,

(C-2) the signal $x$ uniformly distributed on $[-L_x, L_x]$, $0 \le L_u \le L_x$ and $\Delta_y(N-1) \le 2\min\{L_x - L_u, L_u/(M-1)\}$

is satisfied, the optimal added noise with the PDF

$$p_\eta(x) = \begin{cases} \frac{1}{\Delta_y(N-1)}, & x \in [-\frac{\Delta_y(N-1)}{2}, \frac{\Delta_y(N-1)}{2}], \\ 0, & \text{otherwise} \end{cases} \tag{8}$$

corresponds to the minimum MSE. Note that the condition (C-1) places no limitation on the type of signal. Proofs of the optimal noise PDF under the condition (C-1) or (C-2) are shown in Appendix B.

It is seen from Eq. (8) that, for only one quantizer ($N = 1$), the PDF of the optimal noise reduces to the Dirac delta function $\delta(x)$, indicating that the MSE is minimized in the absence of added noise. Thus, the SSR effect does not appear in this case. For the array size $N > 1$, Eq. (8) indicates that the added noise can be beneficial, and the optimal noise is uniformly distributed. Fig. 2 plots the MSE $\log_2(D)$ versus the noise standard deviation $\sigma_\eta$ for different array sizes $N$. Here, the input signal $x = \sin(2\pi t)$, the quantization levels $M = 3$, the bound $L_u = 1$,

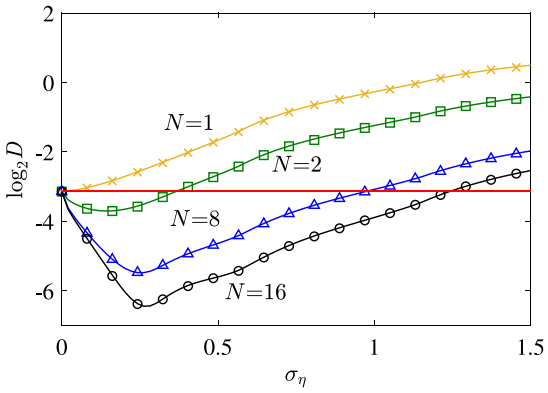


**Fig. 2.** Plots of $\log_2 D$ versus the uniform noise level (standard deviation) $\sigma_\eta$ for different array sizes $N$. Here, $x \sim U[-1,1]$, $M = 3$, $L_u = 1$, $\Delta_u = 1$, $\Delta_y = \Delta_u/N$. The optimal noise PDF indicated in Eq. (8) is employed. The curves (solid lines) are theoretically calculated from Eq. (5), and the numerical results of the model in Fig. 1 achieved by $10^3$ Monte Carlo trials are also plotted for array sizes $N = 1$ (×), 2 (□), 8 (△) and 16 (○).

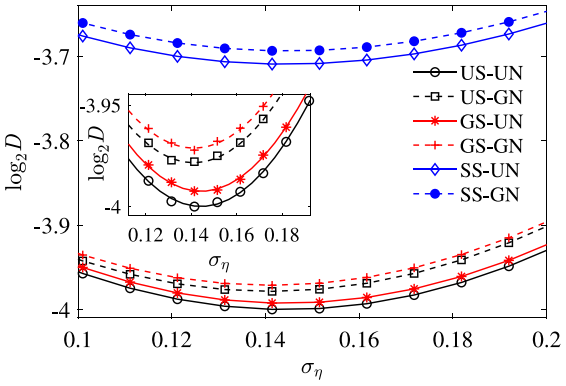


**Fig. 3.** Plots of $\log_2 D$ versus the added noise standard deviation $\sigma_\eta$ for the input signals $x \sim U[-1,1]$ (US), $x \sim \mathbb{N}(0, 1/3)$ (GS) and $x = \sin(2\pi t)$ (SS) buried in uniform noise (UN) and Gaussian noise (GN), respectively. Here, $N = 2$ and other parameters are the same as in Fig. 2. The curves are theoretical results, and the numerical results achieved by Monte Carlo trials are represented by marks.

the decoding steps $\Delta_y = \Delta_u/N = 0.5, 0.1250$ and $0.0625$ for array sizes $N = 2, 8$ and 16, thereby the condition (C-1) holds. Since adding noise will only have a negative effect for a single quantizer ($N = 1$), it is seen in Fig. 2 that the MSE increases monotonically as the noise level $\sigma_\eta$ increases. While, for the quantizer-array ($N > 1$), the MSE distortion versus the noise level $\sigma_\eta$ first decreases and then increases above its initial value. Hence, in this circumstance, the addition of uniform noise with an appropriate noise level $\sigma_\eta$ can greatly reduce the MSE. It is shown in Fig. 2 that, for array sizes $N = 2, 8$ and 16, the corresponding optimal noise levels $\sigma_\eta^{\mathrm{opt}}$ are 0.1443, 0.2526 and 0.2706, respectively. Accordingly, the boundaries of the optimal added noise $L_\eta^{\mathrm{opt}} = \sqrt{3}\sigma_\eta^{\mathrm{opt}} = 0.25$, 0.4375 and 0.4687 respectively, which are exactly equal to $\Delta_y(N-1)/2$ as indicated in Eq. (8). Moreover, the corresponding minimum of MSE gradually decreases as $N$ increases.

For comparison, we choose three different input signals, i.e. uniform signal (US) $x \sim U[-1,1]$, Gaussian signal (GS) $x \sim \mathbb{N}(0, 1/3)$ and sinusoidal signal (SS) $x = \sin(2\pi t)$, and add the uniform noise (UN) or Gaussian noise (GN) into the quantizer-array, respectively. Here, $N = 2$, $M = 3$, $\Delta_u = 1$, and $\Delta_y = \Delta_u/N = 0.5$. It is shown in Fig. 3 that the optimal added uniform noise does lead to a lower MSE than the Gaussian noise for the considered input signals, and the MSE reaches its minima identically at the optimal uniform noise level $\sigma_\eta^{\mathrm{opt}} = 0.1443$. This is because that the optimal added uniform noise accords to the

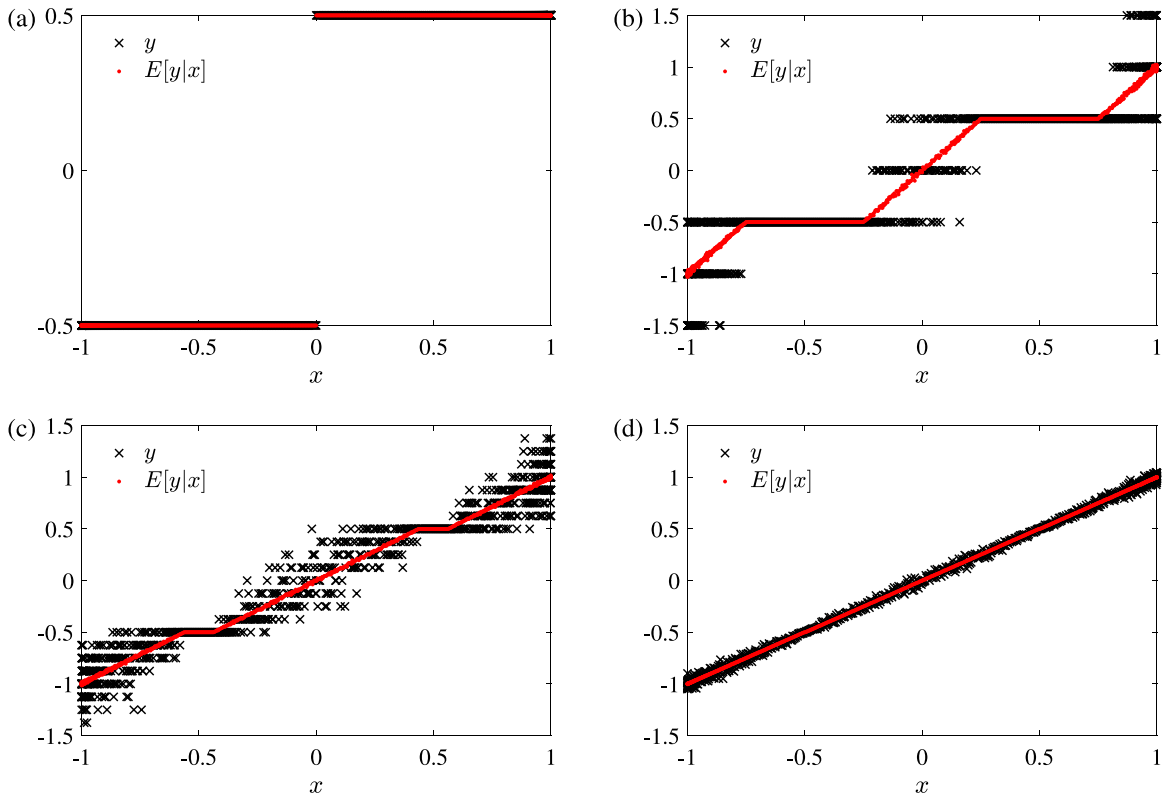


**Fig. 4.** Plots of the output $y$ and the conditional mean $E[y|x]$ for array sizes (a) $N = 1$, (b) $N = 2$, (c) $N = 8$, and (d) $N = 256$. Here, $x = \sin(2\pi t)$, $M = 3$, $\Delta_u = 1$, $\Delta_y = \Delta_u/N$. The optimal uniform noise is with the PDF of Eq. (8). The numerical results of the model in Fig. 1 are obtained by $10^3$ Monte Carlo trials.

distribution $U[-0.25, 0.25]$ for any input signal under the condition (C-1).

It should be mentioned that the output $y$ is a biased estimation when the optimal noise is employed unless $N$ is large enough. To see this, the MSE in Eq. (4) can be decomposed into two parts

$$\begin{aligned} D &= \mathrm{E}\left[(y-x)^2\right] = \mathrm{E}\left[\mathrm{E}\left[y-x\right]^2|x\right] \\ &= \mathrm{E}\left[\mathrm{E}\left[x-\mathrm{E}[y|x]+\mathrm{E}[y|x]-y\right]^2|x\right] \\ &= \mathrm{E}\left[x-\mathrm{E}[y|x]\right]^2 + \mathrm{E}\left[\mathrm{var}[y|x]\right]. \end{aligned} \tag{9}$$

The first part $\mathrm{E}\left[x-\mathrm{E}[y|x]\right]^2$ on the right hand side of Eq. (9) reflects the mean squared bias of the output $y$ given the input $x$, and the second part $\mathrm{E}\left[\mathrm{var}[y|x]\right]$ measures the average variation of the output $y$ given the input $x$. Hence, the degrees of bias and variation together determines the MSE distortion.

Fig. 4 displays the output $y$ and the conditional mean $E[y|x]$ for different array sizes $N$. Note that there is no SSR effect for $N = 1$, and the added noise is not needed. Thus, the output $y$ is determined by the input $x$, and the behaviors of $y$ and $E[y|x]$ overlap totally, as shown in Fig. 4(a). For $N > 1$, the added noise introduces randomness into the quantizer-array. Specifically, for $N = 2$, $E[y|x]$ shows a stair-stepping trend as the input $x$ increases, as illustrated in Fig. 4(b). The output $y$ can take several possible values for some values of the input $x$, leading to linear monotonically stair step traces. Nevertheless, as the range of the optimal uniform noise generated from the range $[-\Delta_y(N-1)/2, \Delta_y(N-1)/2]$ for $N = 2$ is not large enough to make the output $y$ randomized for all the values of $x$, there remain some overlapping parts of $E[y|x]$ and $y$. The difference between $E[y|x]$ and $x$ indicates that the output $y$ is a biased estimation. As the array size $N$ increases, the range of the optimal uniform noise expands, and the overlapping parts of $y$ and $E[y|x]$ shrinkage gradually (see Fig. 4(c)). If $N$ increases further (see Fig. 4(d)), the overlapping parts disappear. In this situation, the conditional expectation $E[y|x]$ almost coincides with the input $x$, and the output $y$ becomes an unbiased estimate.

## 4. Optimal parameters of the designed quantizer-array

In this section, we focus on estimating the uniformly distributed signal $x$ in the range $[-L_x, L_x]$ by the $M$-ary quantizer-array ($M > 1$). Without the added noise, the MSE $D^{\mathrm{NN}}$ can be calculated from Eq. (5) as

$$\begin{aligned} D^{\mathrm{NN}} = &\frac{(M+1)MN\Delta_y L_u^2}{6(M-1)L_x} - \frac{(M+1)MN^2\Delta_y^2 L_u}{6L_x} \\ &+ \frac{N^2M^2\Delta_y^2}{4} - \frac{L_xNM\Delta_y}{2} + \frac{L_x^2}{3}. \end{aligned} \tag{10}$$

By differentiating $D^{\mathrm{NN}}$ with respect to $\Delta_y$ and $L_u$ and letting the partial derivatives be equal to zero, the optimal parameter pair $(\Delta_y^{\mathrm{opt,NN}}, L_u^{\mathrm{opt,NN}})$ can be derived as

$$\Delta_y^{\mathrm{opt,NN}} = \frac{2L_x}{(M+1)N}, \quad L_u^{\mathrm{opt,NN}} = \frac{(M-1)L_x}{M+1}. \tag{11}$$

The optimal quantization level interval $\Delta_u^{\mathrm{opt,NN}}$ can be obtained directly from the optimal boundary of the quantization levels $L_u^{\mathrm{opt,NN}}$ as

$$\Delta_u^{\mathrm{opt,NN}} = \frac{2L_u^{\mathrm{opt,NN}}}{M-1} = \frac{2L_x}{M+1}. \tag{12}$$

Substituting Eq. (11) into Eq. (10) yields the minimum of the MSE

$$D^{\mathrm{opt,NN}} = \frac{L_x^2}{3(M+1)^2}. \tag{13}$$

Now we assume that $\Delta_y$, $L_u$, and $L_x$ satisfy the condition (C-2) so that the optimal noise can be obtained. For $M > 1$, substituting the CDF of the optimal noise into Eq. (5) gives the analytical expression of the MSE

$$\begin{aligned} D = &\frac{(M+1)N\Delta_y M L_u^2}{6(M-1)L_x} - \frac{(M+1)N^2\Delta_y^2 M L_u}{6L_x} - \frac{NM(N-1)^2\Delta_y^3}{24L_x} \\ &+ \frac{N^2M^2\Delta_y^2}{4} - \frac{L_xNM\Delta_y}{2} + \frac{L_x^2}{3}. \end{aligned} \tag{14}$$

From Eq. (17b), the optimal parameter pair $(\Delta_y^{\rm opt}, L_u^{\rm opt})$ are given by

$$\Delta_y^{\rm opt} = \frac{2\left(NM - \sqrt{2N-1}\right)L_x}{N^2(M+1)(M-1)+(N-1)^2}, \tag{15a}$$

$$L_u^{\rm opt} = \frac{N(M-1)\left(NM - \sqrt{2N-1}\right)L_x}{N^2(M+1)(M-1)+(N-1)^2}. \tag{15b}$$

The Hessian matrix of $D$ at $(\Delta_y^{\rm opt}, L_x^{\rm opt})$ can be verified to be positive definite, implying that it is a minimum. The optimal quantization level interval $\Delta_u^{\rm opt}$ can be acquired directly from $L_u^{\rm opt}$ as

$$\Delta_u^{\rm opt} = \frac{2N\left(NM - \sqrt{2N-1}\right)L_x}{N^2(M+1)(M-1)+(N-1)^2}. \tag{16}$$

Correspondingly, the boundary of the optimal uniform noise $L_\eta^{\rm opt}$ as well as the minimum $D^{\rm opt}$ can be achieved as

$$L_\eta^{\rm opt} = \frac{(N-1)\left(NM - \sqrt{2N-1}\right)L_x}{N^2(M+1)(M-1)+(N-1)^2}, \tag{17a}$$

$$D^{\rm opt} = \frac{(2N-1)\left(NM - \sqrt{2N-1}\right)^2 L_x^2}{3\left[N^2(M+1)(M-1)+(N-1)^2\right]^2}. \tag{17b}$$

The results in Eqs. (15) and (17) are compatible with the optimal parameters for $M = 1$ [77]. It is interesting that the relation $\Delta_y = \Delta_u/N$ in the condition (C-1) holds for both $(\Delta_y^{\rm opt}, \Delta_u^{\rm opt})$ and $(\Delta_y^{\rm opt,NN}, \Delta_u^{\rm opt,NN})$.

In the absence of noise, $L_u^{\rm opt,NN}$ and $D_y^{\rm opt,NN}$ are independent of the array size $N$, but $\Delta_y^{\rm opt,NN}$ decreases as $N$ increases. By contrast, when the optimal uniform noise is added, $L_u^{\rm opt}$ increases, while $\Delta_y^{\rm opt}$ and $D^{\rm opt}$ decrease as $N$ increases. The $M$-ary quantizer-array ($M > 1$) displays improved performance over the binary one ($M = 1$) in the sense of minimizing the MSE distortion.

Fixing $M$ and letting $N$ tend to infinity gives $\lim_{N\to+\infty} \Delta_y^{\rm opt} = 0$, $\lim_{N\to+\infty} L_u^{\rm opt} = L_x - L_x/M$, $\lim_{N\to+\infty} L_\eta^{\rm opt} = L_x/M$, and $\lim_{N\to+\infty} D^{\rm opt} = 0$. Thus, for the binary case ($M = 1$), $\lim_{N\to+\infty} L_\eta^{\rm opt} = L_x$, and the optimal noise is identical to the signal. This result is in accordance with the discussion for large array size $N$ in Ref. [32]. For $M > 1$, $\lim_{N\to+\infty} L_\eta^{\rm opt} < L_x$. On the other hand, if $N$ is fixed and $M$ goes to infinity, each quantizer's output is continuous. Then, from Eq. (15), the optimal boundary $L_u^{\rm opt}$ coincides with the signal boundary $L_x$. In this case, $\Delta_y^{\rm opt}$, $L_\eta^{\rm opt}$, and $D^{\rm opt}$ converge to zero regardless of the array size $N$. Thus, adding noise will only degrade the estimation performance of the designed quantizer-array, and the SSR phenomenon disappears.

## 5. Optimal added noise for minimizing MSE distortion in the presence of background noise

It should be noted that the background noise is not considered in the above theoretical investigations. The obtained results on the optimal added noise cannot be extended directly to the situation of the presence of background noise. Here, we discuss the optimal added noise for minimizing MSE distortion of the quantizer-array in two possible cases of background noise: the transmission channel noise (Case A) and the quantizer noise (Case B) (see Fig. 5).

For the Case A, the signal $x$ is corrupted by the background noise $\xi$ in the transmission channel, thus the input of the quantizer-array in Fig. 1 should be replaced by the noisy one $x + \xi$. For mutually independent random variables $x$ and $\xi$ with known distributions, it is proven in Appendix C.1 that the MSE distortion $D$ of the quantizer-array is still a convex functional of the CDF $F_\eta$ of the added noise. Hence, the existence of the optimal added noise $\eta^{\rm opt}$ is guaranteed. However, the PDF $p_{\eta^{\rm opt}}$ of the optimal added noise $\eta^{\rm opt}$ is relevant with the input signal $x$ and the background noise $\xi$. It is not easy to find the closed form expression of $p_{\eta^{\rm opt}}$ in general. The MSE distortion $\log_2 D$ in the presence of different types of background noise is simulated numerically by adding noise to the quantizer-array, and the numerical results are displayed in Fig. 5(a) for comparison. Here, three background noise types of Lévy noise $S_{1.8}(0.05, 0, 0)$ (LBN), uniform noise $U[-0.125, 0.125]$ (UBN) and Gaussian noise $\mathbb{N}(0, 0.05^2)$ (GBN) are considered. Therein, in the notion of Lévy noise $S_\alpha(\sigma, \beta, \mu)$, $\alpha \in (0, 2]$ is the stability index, $\sigma > 0$ is the scale parameter, $\beta \in [-1, 1]$ is the asymmetry parameter and $\mu \in (-\infty, +\infty)$ is the location parameter [12]. The quantizer-array is added by Uniform (UN), Gaussian (GN) and dichotomous noise (DN), respectively. It is seen in Fig. 5(a) that the proper amount of added noise can reduce the MSE distortion for the three types of background noise. However, the added uniform noise achieves the lowest MSE distortion, followed by Gaussian noise and then dichotomous noise. As the optimal added noise type is not established theoretically, we can expect to acquire a lower MSE distortion by other types of added noise than that by three considered noise types.

For the Case B, the quantizer-array contains $N$ background noise components $\xi_i$ for $i = 1, 2, \ldots, N$. We suppose that the background noise components $\xi_i$ are mutually independent identically distributed, and the background noise $\xi_i$ and the added noise $\eta_i$ are also independent. Similarly to the Case A, the MSE distortion is also convex (see Appendix C.2) and thus the optimal added noise $\eta_i^{\rm opt}$ ($i = 1, 2, \ldots, N$) always exists if the distributions of the input signal $x$ and the background noise $\xi_i$ ($i = 1, 2, \ldots, N$) are given. Moreover, if the composite noise $\xi_i + \eta_i^{\rm opt}$ obeys the optimal uniform distribution, i.e.,

$$\xi_i + \eta_i^{\rm opt} \sim U\left[-\frac{\Delta_y(N-1)}{2}, \frac{\Delta_y(N-1)}{2}\right], \tag{18}$$

then the minimal MSE distortion $D^{\rm opt}$ is equal to that in the absence of background noise as displayed in Eq. (17b). In this case, the production of the characteristic functions $C_\xi$ of the background noise $\xi_i$ and $C_{\eta^{\rm opt}}$ of the optimal added noise $\eta_i^{\rm opt}$ satisfies

$$C_\xi(t) C_{\eta^{\rm opt}}(t) = \frac{2}{t}\sin\left(\frac{\Delta_y(N-1)t}{2}\right). \tag{19}$$

The right-hand side of Eq. (19) is the characteristic function of the uniform distribution $U[-\Delta_y(N-1)/2, \Delta_y(N-1)/2]$. Thereby, the characteristic function of the optimal added noise is given by

$$C_{\eta^{\rm opt}}(t) = \frac{2}{tC_\xi(t)}\sin\left(\frac{\Delta_y(N-1)t}{2}\right). \tag{20}$$

Further, the inverse Fourier transformation of Eq. (20) yields the PDF $p_{\eta^{\rm opt}}$ of the optimal added noise if it exists.

For instance, if the background noise $\xi_i$ obeys the uniform distribution in the interval $[-\Delta_y(N-1)/4, \Delta_y(N-1)/4]$ for $i = 1, 2, \ldots, N$, then we can obtain $C_{\eta^{\rm opt}}(t) = 2\cos(\Delta_y(N-1)t/4)$. The corresponding PDF of the optimal added noise $\eta_i^{\rm opt}$ is given by $p_{\eta^{\rm opt}}(x) = 0.5\delta(x-\Delta_y(N-1)t/4) + 0.5\delta(x+\Delta_y(N-1)t/4)$, this is the dichotomous noise.

However, if the background noise is Gaussian or Lévy distributed, the optimal added noise cannot be deduced from Eq. (18). For example, we as well consider the zero-mean symmetric Lévy distribution, whose characteristic function is expressed as [12]

$$C_\xi(t) = e^{-\sigma^\alpha |t|^\alpha} \tag{21}$$

with $\alpha \in (0, 2]$, $\sigma \in [0, +\infty)$. Substituting Eq. (21) into Eq. (20) gives

$$C_{\eta^{\rm opt}}(t) = \frac{2}{t}\sin\left(\frac{\Delta_y(N-1)t}{4}\right)e^{\sigma^\alpha |t|^\alpha}, \tag{22}$$

which diverges as $t$ goes to infinity for any $\alpha \in (0, 2]$. Hence $C_{\eta^{\rm opt}}(t)$ in Eq. (22) cannot be a characteristic function of any distribution, and the optimal added noise that satisfies Eq. (18) does not exist. In this situation, adding proper amount of noise could reduce the MSE distortion to some extent, although it cannot eliminate the effect of background noise and minimizes the MSE distortion in Eq. (17) to the greatest extent. The numerical results of the MSE distortion $\log_2 D$ in the presence of different types of background noise are displayed

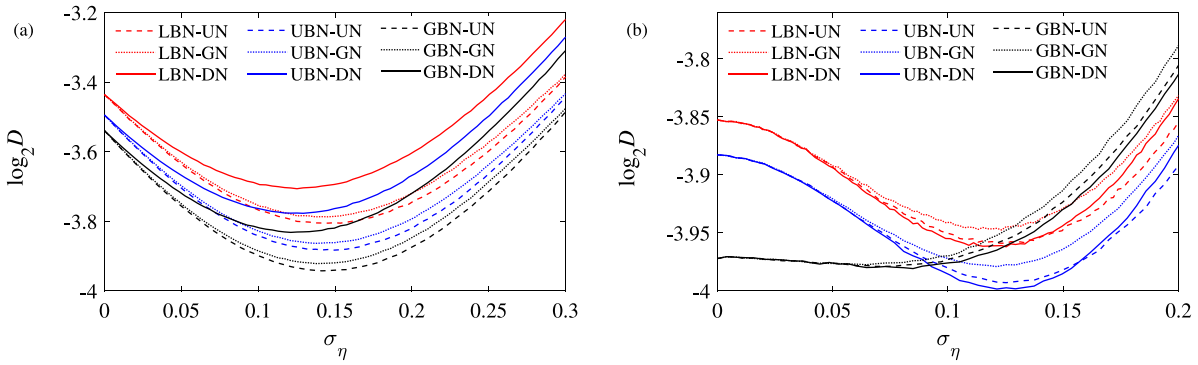


**Fig. 5.** Plots of $\log_2 D$ versus the added noise level (standard deviation) $\sigma_\eta$ for different background noise types in the quantizer-array for the (a) Case A and (b) Case B. Lévy background noise $S_{1.8}(0.05, 0, 0)$ (LBN), uniform background noise $U[-0.125, 0.125]$ (UBN) and Gaussian background noise $\mathbb{N}(0, 0.05^2)$ (GBN) are considered. Uniform (UN), Gaussian (GN) and dichotomous (DN) added noise are employed, respectively. Here, the input signal $x \sim U[-1, 1]$. $M = 3$, $N = 2$, $L_u = 1$, $\Delta_u = 1$, $\Delta_y = \Delta_u/N$. The results are obtained numerically by $10^3$ Monte Carlo trials.

in Fig. 5(a). The considered types of background noise and added noise are the same as in Fig. 5(b). We can see in Fig. 5(b) that, for the uniform background noise $U[-0.125, 0.125]$, the dichotomous noise achieves the lowest MSE among the three types of added noise, and the minimal MSE is reached at the noise intensity $\sigma_\eta = 0.125$. The PDF of the corresponding dichotomous noise can be expressed as $p_\eta(x) = 0.5\delta(x - 0.125) + 0.5\delta(x + 0.125)$. This result accords to the above mentioned theoretical analysis. As $\Delta_y(N - 1)/4 = 0.125$ and under the background noise $U[-0.125, 0.125]$, the optimal added noise is solvable, i.e. the dichotomous noise taking its values $\pm 0.125$ equiprobably. Further, by comparing Figs. 5(b) and 2, we can find that the lowest MSE distortion of the quantizer-array in the presence of the background noise $U[-0.125, 0.125]$ is the same as that in the absence of background noise. The beneficial role of added noise is significantly demonstrated in both cases. The theoretical and numerical results are consistent. It is also shown in Fig. 5(b) that, for the Lévy or Gaussian background noise, the added dichotomous noise performs better than the other two types of added noise, but the corresponding MSE distortion is always larger than that in the absence of background noise (see Fig. 2). As discussed above, since the PDF of the added noise does not satisfy Eq. (18), then the minimal MSE distortion is always larger than that in the absence of background noise.

## 6. Conclusion

In this paper, we theoretically analyze the optimization of $M$-ary SSR in the quantizer-array linear estimation. It is proven that the optimal noise with uniform PDF can achieve the minimum MSE distortion for any input signal if the quantization level interval $\Delta_u$ is $N$ times the decoding step size $\Delta_y$. Furthermore, for a uniformly distributed signal, the optimal uniform added noise also holds as the decoding step size $\Delta_y$, the boundary of quantization levels $L_u$, and the boundary of the signal $L_x$ satisfy a certain inequality constraint. In the latter case, the optimal parameters, including the quantization level interval $\Delta_u^{\text{opt}}$ and linear decoding step size $\Delta_y^{\text{opt}}$, are derived analytically. We finally discuss the optimal added noise for minimizing distortions of the quantizer-array linear estimation in the presence of the background noise.

Besides the exploration of the beneficial effect of noise on SSR, it is also noted that dithering is another noise-enhanced phenomenon in quantizers [78,79]. Although both techniques involve intentionally adding noise to the input signal, the characteristics of the two effects are different in certain ways. The goal of dithering is to make the quantization error, which is the difference between the input signal and the output signal, statistically independent of the input signal [27,80]. Dithering can occur in a single quantizer, but SSR only exists in parallel quantizer-arrays ($N > 1$).

It is interesting to note that the condition (C-1) holds for the optimal parameter pair ($\Delta_y^{\text{opt}}$, $\Delta_u^{\text{opt}}$) and the parameter pair ($\Delta_y^{\text{opt,NN}}$, $\Delta_u^{\text{opt,NN}}$), both obtained under the condition (C-2). Hence, we pose the following open question: Does the optimal $\Delta_y$ and $\tau$ satisfy the condition (C-1) for an arbitrary input signal? If the answer is yes, then we conclude that the added uniform noise can yield the lowest MSE no matter what the input signal is. This interesting question deserves further study. In addition, the decoder is assumed to be linear, and the quantization levels are set to be equally spaced in this study. One might possibly expect improved performance of the quantizer-array if these conditions are relaxed, which is also worthy of further study.

## CRediT authorship contribution statement

**Tianting Xie:** Conceptualization, Methodology, Formal analysis, Software, Writing – original draft. **Yuandong Ji:** Software, Validation, Funding acquisition. **Zhongshan Yang:** Methodology, Supervision. **Fabing Duan:** Methodology, Formal analysis, Writing – review & editing. **Derek Abbott:** Validation, Visualization, Writing – review & editing.

## Declaration of competing interest

The authors declare that they have no known competing financial interests or personal relationships that could have appeared to influence the work reported in this paper.

## Data availability

Data will be made available on request.

## Acknowledgment

This work is sponsored by the National Natural Science Foundation of China (Grant No. 61701329).

## Appendix A. Calculation of $\mathrm{E}[I|x]$ and $\mathrm{E}[I^2|x]$

Noting that each quantizer's output $I_i$ is $i.i.d.$ for $i = 1, 2, \ldots, N$, and we denote $P\{I_i = k|x\}$ as $P_{k|x}$ for short. By definition,

$$P_{k|x} = P\{u_k \le x + \eta_i < u_{k+1}|x\} = F_\eta(u_{k+1} - x) - F_\eta(u_k - x) \tag{A.1}$$

for $k = 0, 1, \ldots, M$. Let $W_k$ be the number of $N$ quantizers whose outputs are equal to $k$. In this case, $W_k \in \{0, 1, \ldots, N\}$, $k = 0, 1, \ldots, M$. Letting $W = (W_0, W_1, \ldots, W_M)$, $W$ obeys a multinomial distribution [81]. Accordingly,

$$\begin{aligned} &\mathrm{E}[W_k|x] = NP_{k|x}, \\ &\mathrm{E}[W_k^2|x] = NP_{k|x} + N(N-1)P_{k|x}^2, \\ &\mathrm{E}[W_kW_j|x] = N(N-1)P_{k|x}P_{j|x}, \quad k \ne j. \end{aligned} \tag{A.2}$$

As $I = \sum_{k=0}^{M} kW_k = \sum_{k=1}^{M} kW_k$, then

$$\begin{aligned}\mathrm{E}[I|x] &= \sum_{k=1}^{M} k\mathrm{E}(W_k|x) = N\sum_{k=1}^{M} kP_{k|x},\\ \mathrm{E}[I^2|x] &= \sum_{k=1}^{M}\sum_{j=1}^{M} kj\mathrm{E}[W_kW_j|x]\\ &= N\sum_{i=1}^{M} k^2P_{k|x} + N(N-1)\sum_{k=1}^{M}\sum_{j=1}^{M} kjP_{k|x}P_{j|x}.\end{aligned} \tag{A.3}$$

Substituting Eq. (A.1) into Eq. (A.3) yields

$$\mathrm{E}[I|x] = NM - N\sum_{k=1}^{M} F_\eta(u_k - x), \tag{A.4}$$

$$\begin{aligned}\mathrm{E}[I^2|x] = {} & NM^2 + N\sum_{k=1}^{M}(1-2k)F_\eta(u_k-x)\\ & + N(N-1)\left[\sum_{k=1}^{M} F_\eta(u_k-x) - M\right]^2.\end{aligned} \tag{A.5}$$

## Appendix B. Proof of the optimal noise

### B.1. Necessary condition of the optimal noise

The CDF of the optimal added noise $F_\eta^{\mathrm{opt}}$ must satisfy

$$\frac{\mathrm{d}}{\mathrm{d}\alpha} D\left[F_\eta^{\mathrm{opt}} + \alpha(F_{\eta'} - F_\eta^{\mathrm{opt}})\right]\Big|_{\alpha=0} \geqslant 0 \tag{B.1}$$

for any $F_{\eta'} \in \mathscr{F}$, based on the necessary condition for the minimum point(s) of a convex functional [77,82]. Thereby,

$$\begin{aligned}&\frac{\mathrm{d}}{\mathrm{d}\alpha} D\left[F_\eta^{\mathrm{opt}} + \alpha(F_{\eta'} - F_\eta^{\mathrm{opt}})\right]\Big|_{\alpha=0}\\ &= \Delta_y N\int_{-\infty}^{+\infty} p_x(x)\left\{\sum_{k=1}^{M}\left[F_{\eta'}(u_k-x) - F_\eta^{\mathrm{opt}}(u_k-x)\right]Z_k(x)\right\}\mathrm{d}x\\ &= \Delta_y N\sum_{k=1}^{M}\int_{-\infty}^{+\infty} p_x(x)\left[F_{\eta'}(u_k-x) - F_\eta^{\mathrm{opt}}(u_k-x)\right]Z_k(x)\mathrm{d}x\\ &= \Delta_y N\sum_{k=1}^{M}\int_{-\infty}^{+\infty} p_x(x)A_k(x;F_{\eta'},F_\eta)\mathrm{d}x \geqslant 0,\end{aligned} \tag{B.2}$$

where

$$\begin{aligned}Z_k(x) &= 2(x-y_0) + \Delta_y(1-2k) - 2\Delta_y(N-1)\sum_{j=1}^{M} j\left[F_\eta^{\mathrm{opt}}(u_{j+1}-x)\right.\\ &\quad \left. - F_\eta^{\mathrm{opt}}(u_j-x)\right],\\ A_k(x;F_{\eta'},F_\eta) &= \left[F_{\eta'}(u_k-x) - F_\eta(u_k-x)\right]Z_k(x), k = 1,2,\ldots,M.\end{aligned} \tag{B.3}$$

### B.2. Proof of the optimal noise under the condition (C-1)

**Proof.** Firstly, we show that the added noise with the PDF of Eq. (8) satisfies the above necessary condition (B.2). We obtain

$$F_\eta(u_k-x) = \begin{cases} 1, & x < u_k - \frac{\Delta_y(N-1)}{2},\\ \frac{u_k-x}{\Delta_y(N-1)} + \frac{1}{2}, & u_j - \frac{\Delta_y(N-1)}{2} \leq x < u_k + \frac{\Delta_y(N-1)}{2},\\ 0, & x \geq u_k + \frac{\Delta_y(N-1)}{2},\end{cases} \tag{B.4}$$

from the CDF of the uniform noise $F_\eta$. Note that $\Delta_u = \Delta_y N > \Delta_y(N-1)$. Hence, for $x \in \left[u_k - \Delta_y(N-1)/2, u_k + \Delta_y(N-1)/2\right]$,

$$F_\eta(u_j-x) = \begin{cases} 1, & j < k,\\ \frac{u_k-x}{\Delta_y(N-1)} + \frac{1}{2}, & j = k,\\ 0, & j > k.\end{cases} \tag{B.5}$$

Substituting Eq. (B.5) into Eq. (B.3) yields $Z_k(x) = 0$ on $\left[u_k - \Delta_y(N-1)/2, u_k + \Delta_y(N-1)/2\right]$. The sign of $Z_k(x)$ on $(-\infty,+\infty)$ can then be identified as follows due to its monotonicity:

$$Z_k(x) = \begin{cases} <0, & x < u_k - \frac{\Delta_y(N-1)}{2},\\ 0, & u_k - \frac{\Delta_y(N-1)}{2} \leq x \leq u_k + \frac{\Delta_y(N-1)}{2},\\ >0, & x > u_k + \frac{\Delta_y(N-1)}{2}.\end{cases} \tag{B.6}$$

Eqs. (B.4) and (B.6) imply that

$$A_k(x;F_{\eta'},F_\eta) \geq 0, \tag{B.7}$$

and thus

$$p_x(x)A_k(x;F_{\eta'},F_\eta) \geq 0. \tag{B.8}$$

Therefore, the above $F_\eta$ satisfies the necessary condition (B.2).

Next, we prove by reduction that the above $F_\eta$ is a minimum. Otherwise, assuming that $F_{\eta'} \in \mathscr{F}$ is a minimum, and $D(F_{\eta'}) < D(F_\eta)$. Due to the convexity of $D(F_\eta)$, for any $\alpha \in (0,1)$,

$$\begin{aligned}D[\alpha F_{\eta'} + (1-\alpha)F_\eta] &\leq \alpha D(F_{\eta'}) + (1-\alpha)D(F_\eta)\\ &< \alpha D(F_\eta) + (1-\alpha)D(F_\eta) = D(F_\eta).\end{aligned} \tag{B.9}$$

Thus, $D[F_\eta + \alpha(F_{\eta'} - F_\eta)] - D(F_\eta) = D[\alpha F_{\eta'} + (1-\alpha)F_\eta] - D(F_\eta) < 0$, which implies that $\frac{\mathrm{d}}{\mathrm{d}\alpha} D\left[F_\eta + \alpha(F_{\eta'} - F_\eta)\right]\Big|_{\alpha=0} \leq 0$.

On the other hand, since $F_\eta$ satisfies the in Eq. (B.2) and equivalently (B.1), then

$$\frac{\mathrm{d}}{\mathrm{d}\alpha} D\left[F_\eta + \alpha(F_{\eta'} - F_\eta)\right]\Big|_{\alpha=0} = 0. \tag{B.10}$$

It can be easily verified from Eq. (5) that $D[F_\eta + \alpha(F_{\eta'} - F_\eta)]$ is a convex quadratic function of $\alpha$ if $F_\eta$ and $F_{\eta'}$ are fixed. Thus, Eq. (B.10) means that $D[F_\eta + \alpha(F_{\eta'} - F_\eta)]$ achieves its minimum at $\alpha = 0$. However, since $F_{\eta'}$ is the minimum point, $D[F_\eta + \alpha(F_{\eta'} - F_\eta)]$ should achieve its minimum at $\alpha = 1$ rather than $\alpha = 0$, which results in a contradiction. Therefore, the above $F_\eta$ is a minimum. □

### B.3. Proof of the optimal noise under the condition (C-2)

**Proof.** We assume that the added noise with the PDF of Eq. (8) is employed, and the condition (C-2) is satisfied. The following three properties of $Z_j(x)$ can be easily verified. For $x \in [-L_x, L_x]$,

Property 1: $Z_k(x) = -Z_{M-k+1}(-x)$, $k = 1,2,\ldots,M$,
Property 2: $Z_k(x)$ is a monotonically increasing function of $x$, $k = 1,2,\ldots,M$,
Property 3: $Z_k(x) = Z_{k-1}(x) - 2\Delta_y$, $k = 2,3,\ldots,M$.

As for the proof of Property 1,

$$F_\eta(u_j-x) + F_\eta(u_{M-j+1}+x) \equiv 1, j = 1,2,\ldots,M, \tag{B.11}$$

yields

$$\sum_{j=1}^{M} F_\eta(u_j+x) + \sum_{j=1}^{M} F_\eta(u_j-x) \equiv M. \tag{B.12}$$

Hence, $Z_k(x)+Z_{M-k+1}(-x)\equiv 0$, i.e., $Z_k(x)=-Z_{M+1-k}(-x)$. Property 2 can be derived by examining the sign of the slope of $Z_k(x)$. Property 3 can be obtained directly from Eq. (B.3).

Based on the above properties, we have:

(1) If $Z_k(x) > 0$ for $x \in [-L_x, L_x]$, then $Z_{M+1-k}(x) < 0$ for $x \in [-L_x, L_x]$. Similarly, if $Z_k(x) < 0$ for $x \in [-L_x, L_x]$, then $Z_{M+1-k}(x) > 0$ for $x \in [-L_x, L_x]$.

(2) If $Z_k(x)$ has a zero point $x_{k,0}$ on $[-L_x, L_x]$, i.e., $Z_k(x_{k,0}) = 0$, $x_{k,0} \in [-L_x, L_x]$, then $Z_{M+1-k}(x)$ also has a zero point $x_{M+1-k,0}$ on $[-L_x, L_x]$ satisfying $x_{M+1-k,0} = -x_{k,0}$. Moreover, $x_{k,0} < 0$ for $k < (M+1)/2$ and $x_{k,0} > 0$ for $k > (M+1)/2$.

In particular, if $M$ is odd, we have $Z_{(M+1)/2}(x) = 0, x \in \left[u_{(M+1)/2} - \Delta_y(N-1)/2, u_{(M+1)/2} + \Delta_y(N-1)/2\right]$. Then

$$A_{(M+1)/2}(x; F_{\eta'}, F_\eta) \geq 0, \tag{B.13}$$

for any $F_{\eta'} \in \mathscr{F}$ and $x \in [-L_x, L_x]$. Thereby,

$$\int_{-L_x}^{L_x} p_x(x) A_{(M+1)/2}(x; F_{\eta'}, F_\eta)\mathrm{d}x \geq 0. \tag{B.14}$$

Thus, we need only discuss the cases of $k < (M+1)/2$ and $k > (M+1)/2$.

As the signal $x \sim U[-L_x, L_x]$,

$$\int_{-\infty}^{+\infty} p_x(x) A_k(x; F_{\eta'}, F_\eta)\mathrm{d}x = \int_{-L_x}^{L_x} p_x(x) A_k(x; F_{\eta'}, F_\eta)\mathrm{d}x \tag{B.15}$$

for $k = 1, 2, \ldots, M$. We divide the range $[-L_x, L_x]$ into four parts based on the above properties. By discussing the signs of the integrals on each part, we show that $F_\eta$ satisfies the necessary condition (B.2). Let

$$x_{k,p} = \begin{cases} -L_x, & \text{if } Z_k(x) > 0, \quad x \in [-L_x, L_x], \\ x_{k,0}, & \text{if } x_{k,0} \text{ exists}, \quad x_{k,0} \in [-L_x, L_x], \\ L_x, & \text{if } Z_k(x) < 0, \quad x \in [-L_x, L_x]. \end{cases} \tag{B.16}$$

If $x_{k,0}$ exists, then

$$\begin{aligned} x_{k,0} &< u_k - \Delta_y(N-1)/2, \quad \text{for} \quad k < (M+1)/2, \\ x_{k,0} &> u_k + \Delta_y(N-1)/2, \quad \text{for} \quad k > (M+1)/2. \end{aligned} \tag{B.17}$$

Hence, the range of the $k$th integral is divided into four parts $R_{k,1}$, $R_{k,2}$, $R_{k,3}$, and $R_{k,4}$:

(1) For $k < (M+1)/2$,

- $R_{k,1}$: $[-L_x, x_{k,p})$,
- $R_{k,2}$: $\left[x_{k,p}, u_k - \frac{\Delta_y(N-1)}{2}\right)$,
- $R_{k,3}$: $\left[u_k - \frac{\Delta_y(N-1)}{2}, u_k + \frac{\Delta_y(N-1)}{2}\right)$,
- $R_{k,4}$: $\left[u_j + \frac{\Delta_y(N-1)}{2}, L_x\right]$,

(2) For $k > (M+1)/2$,

- $R_{k,1}$: $[-L_x, u_k - \frac{\Delta_y(N-1)}{2})$,
- $R_{k,2}$: $\left[u_k - \frac{\Delta_y(N-1)}{2}, u_k + \frac{\Delta_y(N-1)}{2}\right)$,
- $R_{k,3}$: $\left[u_k + \frac{\Delta_y(N-1)}{2}, x_{k,p}\right)$,
- $R_{k,4}$: $\left[x_{k,p}, L_x\right]$.

The signs of the integrals in Eq. (B.15) on $R_{k,1}$, $R_{k,2}$, $R_{k,3}$, and $R_{k,4}$ are discussed as follows.

(1) For $k = 1, 2, \ldots, M$, $x \in R_{k,1}$ or $x \in R_{k,4}$, we have

$$\begin{aligned} &F_\eta(u_k - x) = 1 \quad \text{and} \quad Z_k(x) \leq 0 \quad \text{if} \quad x \in R_{k,1}, \\ &F_\eta(u_k - x) = 0 \quad \text{and} \quad Z_k(x) \geq 0 \quad \text{if} \quad x \in R_{k,4}. \end{aligned} \tag{B.18}$$

Then, $A_k(x; F_{\eta'}, F_\eta) \geq 0$. Consequently, for any $F_{\eta'} \in \mathscr{F}$,

$$\begin{aligned} &\int_{R_{k,1}} p_x(x) A_k(x; F_{\eta'}, F_\eta)\mathrm{d}x \geq 0, \\ &\int_{R_{k,4}} p_x(x) A_k(x; F_{\eta'}, F_\eta)\mathrm{d}x \geq 0. \end{aligned} \tag{B.19}$$

(2) For $k < (M+1)/2$ and $x \in R_{k,2}$,

$$F_\eta(u_k - x) = 1 \quad \text{and} \quad Z_k(x) \geq 0. \tag{B.20}$$

Hence, $A_k(x; F_{\eta'}, F_\eta) \leq 0$. Subsequently,

$$\int_{R_{k,2}} p_x(x) A_k(x; F_{\eta'}, F_\eta)\mathrm{d}x \leq 0 \tag{B.21}$$

for any $F_{\eta'} \in \mathscr{F}$. Nonetheless, we have $x + (M+1-2k)\Delta_u \in \left[x_{k,p} + (M+1-2k)\Delta_u, u_{M+1-k} - \Delta_y(N-1)/2\right]$, which belongs to $R_{M+1-k,1}$. Moreover,

$$\begin{aligned} &Z_{M+1-k}\left(x + (M+1-2k)\,\Delta_u\right) \leq -Z_k(x) \leq 0, \\ &F_{\eta'}\left(u_{M+1-k} - x - (M+1-2k)\Delta_u\right) \\ &- F_\eta\left(u_{M+1-k} - x - (M+1-2k)\Delta_u\right) \\ &= F_{\eta'}(u_k - x) - F_\eta(u_k - x). \end{aligned} \tag{B.22}$$

Consequently,

$$A_{M+1-k}(x + (M+1-2k)\Delta_u; F_{\eta'}, F_\eta) \geq -A_k(x; F_{\eta'}, F_\eta). \tag{B.23}$$

Therefore,

$$\begin{aligned} &\int_{R_{k,2}} p_x(x) A_k(x; F_{\eta'}, F_\eta)\mathrm{d}x \\ &\quad + \int_{R_{M+1-k,1}} p_x(x) A_{M+1-k}(x; F_{\eta'}, F_\eta)\mathrm{d}x \geq 0. \end{aligned} \tag{B.24}$$

Similarly, for $k > (M+1)/2$ and $x \in R_{k,3}$, we have

$$\begin{aligned} &\int_{R_{k,3}} p_x(x) A_k(x; F_{\eta'}, F_\eta)\mathrm{d}x \\ &+ \int_{R_{M+1-k,4}} p_x(x) A_{M+1-k}(x; F_{\eta'}, F_\eta)\mathrm{d}x \geq 0. \end{aligned} \tag{B.25}$$

(3) For $k < (M+1)/2$ and $x \in R_{k,3}$,

$$Z_k(x) = (M+1-2k)\Delta_y N + 2u_k, \tag{B.26}$$

$$x + (M+1-2k)\Delta_u \in R_{M+1-k,2}, \tag{B.27}$$

$$Z_{M+1-k}(x + (M+1-2k)\Delta_u) = -Z_k(x). \tag{B.28}$$

Hence,

$$\begin{aligned} &Z_k(x) \geq 0, \\ &Z_{M+1-k}(x + (M+1-2k)\Delta_u) \leq 0, \\ &Z_k(x) + Z_{M+1-k}(x + (M+1-2k)\Delta_u) = 0. \end{aligned} \tag{B.29}$$

As a result,

$$\begin{aligned} &\int_{R_{k,3}} p_x(x) A_k(x; F_{\eta'}, F_\eta)\mathrm{d}x \\ &\quad + \int_{R_{M+1-k,2}} p_x(x) A_{M+1-k}(x; F_{\eta'}, F_\eta)\mathrm{d}x = 0. \end{aligned} \tag{B.30}$$

Above all, the necessary condition (B.2) holds for $\eta_i \sim U[-\Delta_y(N-1)/2, \Delta_y(N-1)/2]$, $i = 1, 2, \ldots, N$. The rest of the proof is the same as in Appendix B.2. □

## Appendix C. Proof of the convexity of the MSE distortion in the presence of background noise

### C.1. Proof for the Case A

**Proof.** In this case, the MSE distortion in Eq. (4) should be modified as

$$\begin{aligned} D &= \mathrm{E}\left[(y-x)^2\right] \\ &= \int_{-\infty}^{+\infty}\int_{-\infty}^{+\infty}\int_{-\infty}^{+\infty} p_x(x)p_\xi(\xi)p_{y|x,\xi}(y|x,\xi)(y-x)^2 \mathrm{d}y\mathrm{d}\xi\mathrm{d}x \\ &= \int_{-\infty}^{+\infty}\int_{-\infty}^{+\infty} p_x(x)p_\xi(\xi)\left\{\sum_{k=0}^{NM} P\{I=k|x,\xi\}\,[h(k)-x]^2\right\}\mathrm{d}\xi\mathrm{d}x \\ &= \int_{-\infty}^{+\infty}\int_{-\infty}^{+\infty} p_x(x)p_\xi(\xi) \\ &\quad\times\left\{\Delta_y^2\mathrm{E}[I^2|x,\xi] + 2\Delta_y(y_0-x)\mathrm{E}[I|x,\xi] + (y_0-x)^2\right\}\mathrm{d}\xi\mathrm{d}x, \end{aligned} \tag{C.1}$$

where

$$\mathrm{E}[I|x,\xi] = NM - N\sum_{k=1}^{M} F_\eta(u_k - x - \xi) \tag{C.2}$$

and

$$\begin{aligned} \mathrm{E}[I^2|x,\xi] &= NM^2 + N\sum_{k=1}^{M}(1-2k)F_\eta(u_k-x-\xi) \\ &\quad + N(N-1)\left[\sum_{k=1}^{M} F_\eta(u_k-x-\xi) - M\right]^2. \end{aligned} \tag{C.3}$$

For any $\alpha \in [0,1]$ and $F_\eta$, $F_{\eta'} \in \mathscr{F}$, it is easy to verify that $\alpha F_\eta + (1-\alpha)F_{\eta'} \in \mathscr{F}$, indicating that $\mathscr{F}$ is a convex set. Then the convexity of $D(F_\eta)$ is derived immediately by replacing $x$ by $x+\xi$ in Eq. (C.6). □

### C.2. Proof for the case B

**Proof.** The MSE in Eq. (5) should be modified as

$$\begin{aligned} D = \int_{-\infty}^{+\infty} p_x(x) &\left\{ \Delta_y^2 N(N-1)\left[\sum_{k=1}^{M} F_{\xi+\eta}(u_k-x) - M\right]^2 \right. \\ &+ \Delta_y N\sum_{k=1}^{M} F_{\xi+\eta}(u_k-x)\left[\Delta_y - 2\Delta_y k - 2y_0 + 2x\right] \\ &\left. + 2NM\Delta_y(y_0-x) + (y_0-x)^2 + \Delta_y^2 NM^2 \right\}\mathrm{d}x, \end{aligned} \tag{C.4}$$

where

$$\begin{aligned} F_{\xi+\eta}(u_k-x) &= \int_{-\infty}^{+\infty} p_\xi(\xi)\int_{-\infty}^{u_k-x-\xi} p_\eta(\eta)\mathrm{d}\eta\mathrm{d}\xi \\ &= \int_{-\infty}^{+\infty} p_\xi(\xi)F_\eta(u_k-x-\xi)\mathrm{d}\xi. \end{aligned} \tag{C.5}$$

For any $\alpha \in [0,1]$ and $F_\eta$, $F_{\eta'} \in \mathscr{F}$, $\alpha F_\eta + (1-\alpha)F_{\eta'} \in \mathscr{F}$, indicating that $\mathscr{F}$ is a convex set.

$$\begin{aligned} &D\left[\alpha F_\eta + (1-\alpha)F_{\eta'}\right] - \left[\alpha D(F_\eta) + (1-\alpha)D(F_{\eta'})\right] \\ &= \Delta_y^2 N(N-1)\int_{-\infty}^{+\infty} p_x(x)\left\{ -\alpha\left[\sum_{k=1}^{M} F_{\xi+\eta}(u_k-x-\xi) - M\right]^2 \right. \\ &\quad \left. -(1-\alpha)\left[\sum_{k=1}^{M} F_{\xi+\eta'}(u_k-x-\xi) - M\right]^2 \right. \\ &\quad \left. + \left\{\sum_{k=1}^{M}\left[\alpha F_{\xi+\eta}(u_k-x-\xi) + (1-\alpha)F_{\xi+\eta'}(u_k-x-\xi)\right] - M\right\}^2 \right\}\mathrm{d}x \\ &= \Delta_y^2 N(N-1)\alpha(\alpha-1)\int_{-\infty}^{+\infty} p_x(x) \\ &\quad\times\left\{\int_{-\infty}^{+\infty} p_\xi(\xi)\sum_{k=1}^{M}\left[F_\eta(u_k-x-\xi) - F_{\eta'}(u_k-x-\xi)\right]\mathrm{d}\xi\right\}^2\mathrm{d}x \\ &\quad \le 0. \end{aligned} \tag{C.6}$$

Hence, $D(F_\eta)$ is a convex functional defined on $\mathscr{F}$. □

## References


[1] Lanzara E, Mantegna RN, Spagnolo B, Zangara R. Experimental study of a nonlinear system in the presence of noise: The stochastic resonance. Amer J Phys 1997;65:341–9.

[2] Benzi R, Sutera A, Vulpiani A. The mechanism of stochastic resonance. J Phys A: Math Gen 1981;14(11):L453–7.

[3] Wiesenfeld K, Moss F. Stochastic resonance and the benefits of noise - from ice ages to crayfish and squids. Nature 1995;373(6509):33–6.

[4] McDonnell MD, Ward LM. The benefits of noise in neural systems: bridging theory and experiment. Nat Rev Neurosci 2011;12(7):415–25.

[5] Carollo A, Spagnolo B, Dubkov AA, Valenti D. On quantumness in multi-parameter quantum estimation. J Stat Mech Theory Exp 2019;2019:094010.

[6] Bohorquez J, Lambert MF, Alexander B, Simpson AR, Abbott D Derek. Stochastic resonance enhancement for leak detection in pipelines using fluid transients and convolutional neural networks. J Water Resour Plan Manage 2022;148(3):04022001.

[7] Cavagna A, Cimarelli A, Giardina I, Parisi G, Santagati R, Stefanini F, Viale M. Scale-free correlations in starling flocks. Proc Natl Acad Sci 2010;107(26):11865–70.

[8] Nobel prize outreach AB [Internet]. Stockholm: The Outreach, c2022 [cited 2022 Oct 28]. Press release: The Nobel Prize in Physics 2021. Available from: https://www.nobelprize.org/prizes/physics/2021/press-release/.

[9] Lindner B, Garcła-Ojalvo J, Neiman A, Schimansky-Geier L. Effects of noise in excitable systems. Phys Rep 2004;392(6):321–424.

[10] Pizzolato N, Fiasconaro A, Adorno DP, Spagnolo B. Resonant activation in polymer translocation: new insights into the escape dynamics of molecules driven by an oscillating field. Phys Biol 2010;7(3):034001.

[11] Ushakov YV, Dubkov AA, Spagnolo B. Spike train statistics for consonant and dissonant musical accords in a simple auditory sensory model. Phys Rev E 2010;81(4):041911.

[12] Guarcello C, Valenti D, Carollo A, Spagnolo B. Effects of Lévy noise on the dynamics of sine-Gordon solitons in long Josephson junctions. J Stat Mech Theory Exp 2016;2016(5):054012.

[13] Carollo A, Valenti D, Spagnolo B. Geometry of quantum phase transitions. Phys Rep 2020;838:1–72.

[14] Guo Y, Yao T, Wang L, Tan J. Lévy noise-induced transition and stochastic resonance in a tumor growth model. Appl Math Model 2021;94:506–15.

[15] Fiasconaro A, Mazo JJ, Spagnolo B. Noise-induced enhancement of stability in a metastable system with damping. Phys Rev E 2010;82:041120.

[16] Guarcello C, Valenti D Davide, Carollo A, Spagnolo B. Stabilization effects of dichotomous noise on the lifetime of the superconducting state in a long josephson junction. Entropy 2015;17:2862–75.

[17] Agudov NV, Safonov AV, Krichigin AV, Kharcheva AA, Dubkov AA, Valenti D, Guseinov DV, Belov AI, Mikhaylov AN, Carollo A, Spagnolo B. Nonstationary distributions and relaxation times in a stochastic model of memristor. J Stat Mech Theory Exp 2020;2:024003.

[18] Mantegna RN, Spagnolo B. Probability distribution of the residence times in periodically fluctuating metastable systems. Int J Bifurcation Chaos 1998;8(4):783–90.

[19] Stocks NG, Mannella R. Generic noise-enhanced coding in neuronal arrays. Phys Rev E 2001;64(3):030902.

[20] Bayram S, Gezici S. Noise enhanced M-ary composite hypothesis-testing in the presence of partial prior information. IEEE Trans Signal Process 2011;59(3):1292–7.

[21] Chapeau-Blondeau F, Rousseau D. Noise-aided SNR amplification by parallel arrays of sensors with saturation. Phys Lett A 2006;351(4–5):231–7.

[22] Nakashima Y, Yamazato T, Arai S, Tanaka H, Tadokoro Y. Noise-aided demodulation with one-bit comparator for multilevel pulse-amplitude-modulated signals. IEEE Wirel Commun Lett 2018;7(5):848–51.

[23] McDonnell MD, Iannella N, To MS, Tuckwell HC, Henry C, Jost J, Gutkin BS, Ward LM. A review of methods for identifying stochastic resonance in simulations of single neuron models. Network: Comput Neural Syst 2015;26(2):35–71.

[24] Filatov DO, Vrzheshch DV, Tabakov OV, Novikov AS, Belov AI, Antonov ININ, Sharkov VV, Koryazhkina MN, Mikhaylov AN, Gorshkov ON, Dubkov AA, Carollo A, Spagnolo B. Noise-induced resistive switching in a memristor based on $ZrO_2(Y)/Ta_2O_5$ stack. J Stat Mech Theory Exp 2019;2019:124026.

[25] Yakimov AV, Filatov DO, Gorshkov ON, Antonov DA, Liskin DA, Antonov IN, Belyakov AV, Klyuev AV, Carollo A, Spagnolo B. Measurement of the activation energies of oxygen ion diffusion in yttria stabilized zirconia by flicker noise spectroscopy. Appl Phys Lett 2019;114:253506.

[26] Mikhaylov AN, Guseinov DVDV, Belov AI, Korolev DS, Shishmakova VA, Koryazhkina MN, Filatov DO, Gorshkov ON, Maldonado D, Alonso FJ, Roldán JB, Krichigin AV, Agudov NV, Dubkov AA, Carollo A, Spagnolo B. Stochastic resonance in a metal-oxide memristive device. Chaos Solitons Fractals 2021;144:110723.

[27] McDonnell MD, Abbott D. What is stochastic resonance? Definitions, misconceptions, debates, and its relevance to biology. PLoS Comput Biol 2009;5(5):e1000348.

[28] Lisowski B, Valent D, Spagnolo B, Bier M, Gudowska-Nowak E. Stepping molecular motor amid Lévy white noise. Phys Rev E 2015;91:042713.

[29] Valenti D, Schimansky-Geier L, Sailer X, Spagnolo B. Moment equations for a spatially extended system of two competing species. Eur Phys J B 2006;50(1–2):199–203.

[30] Park JI, Kim BJ, Park HJ. Stochastic resonance of abundance fluctuations and mean time to extinction in an ecological community. Phys Rev E 2021;104:024133.

[31] Nguyen T. Robust data-optimized stochastic analog-to-digital converters. IEEE Trans Signal Process 2007;55(6):2735–40.

[32] McDonnell MD, Stocks NG, Pearce CEM, Abbott D. Stochastic resonance: From suprathreshold stochastic resonance to stochastic signal quantization. Cambridge: Cambridge University Press; 2008.

[33] Lu S, He Q, Wang J. A review of stochastic resonance in rotating machine fault detection. Mech Syst Signal Process 2019;116:230–60.

[34] Morse RP, Morse PF, Nunn TB, Archer KAM, Boyle P. The effect of Gaussian noise on the threshold, dynamic range, and loudness of analogue cochlear implant stimuli. J Assoc Res Otolaryngol 2007;8(1):42–53.

[35] McDonnell MD, Amblard P, Stocks NG. Stochastic pooling networks. J Stat Mech Theory Exp 2009;P01012.

[36] Jung P, Hänggi P. Amplification of small signals via stochastic resonance. Phys Rev A 1991;44(12):8032–42.

[37] Wang Y, Wu L. Nonlinear signal detection from an array of threshold devices for non-Gaussian noise. Digit Signal Process 2007;17(1):76–89.

[38] Gao FY, Kang YM, Chen X, Chen G. Fractional Gaussian noise-enhanced information capacity of a nonlinear neuron model with binary signal input. Phys Rev E 2018;97:052142.

[39] Dybiec B. Lévy noises: double stochastic resonance in a single-well potential. Phys Rev E 2009;80:041111.

[40] Mantegna RN, Spagnolo B, Testa L, Trapanese M. Stochastic resonance in magnetic systems described by Preisach hysteresis model. J Appl Phys 2005;97:10E519.

[41] Badzey RL, Mohanty P. Coherent signal amplification in bistable nanomechanical oscillators by stochastic resonance. Nature 2005;437(7061):995–8.

[42] Perc M. Stochastic resonance on paced genetic regulatory small-world networks: effects of asymmetric potentials. Eur Phys J B 2009;69(1):147–53.

[43] Zhang W, Shi P, Li M, Han D. A novel stochastic resonance model based on bistable stochastic pooling network and its application. Chaos Solitons Fractals 2021;145:110800.

[44] Stocks NG. Suprathreshold stochastic resonance in multilevel threshold systems. Phys Rev Lett 2000;84(11):2310–3.

[45] Stocks NG. Information transmission in parallel threshold arrays: Suprathreshold stochastic resonance. Phys Rev E 2001;63(4):041114.

[46] Wannamaker RA, Lipshitz SP, Vanderkooy J. A theory of non-subtractive dither. IEEE Trans Signal Process 2000;48(2):499–516.

[47] Chatterjee M, Oba SI. Noise improves modulation detection by cochlear implant listeners at moderate carrier levels. J Acoust Soc Am 2005;118(2):993–1002.

[48] Rousseau D, Chapeau-Blondeau F. Constructive role of noise in signal detection from parallel arrays of quantizers. Signal Process 2005;85:571–80.

[49] Yang T, Liu S, Liu H, Yang S, Li Y. Stochastic resonance benefits in signal detection under MAP criterion. Commun Nonlinear Sci Numer Simul 2021;102:105919.

[50] Durrant S, Kang Y, Stocks N, Feng J. Suprathreshold stochastic resonance in neural processing tuned by correlation. Phys Rev E 2011;84(1):011923.

[51] Yonekura S, Kuniyoshi Y, Kawaguchi Y. Growth of stochastic resonance in neuronal ensembles with the input signal intensity. Phys Rev E 2012;86(1):011922.

[52] Yilmaz E, Uzuntarla M, Ozer M, Perc M. Stochastic resonance in hybrid scale-free neuronal networks. Physica A 2013;392(22):5735–41.

[53] Wang J, Guo X, Yu H, Liu C, Deng B, Wei X, Chen Y. Stochastic resonance in small-world neuronal networks with hybrid electrical-chemical synapses. Chaos Solitons Fractals 2014;60:40–8.

[54] Guo D, Perc M, Zhang Y, Xu P, Yao D. Frequency-difference-dependent stochastic resonance in neural systems. Phys Rev E 2017;96(2):022415.

[55] Guo D, Perc M, Liu T, Yao D. Functional importance of noise in neuronal information processing. Europhys Lett 2018;124:50001.

[56] Kawaguchi M, Mino H, Durand DM. Stochastic resonance can enhance information transmission in neural networks. IEEE Trans Biomed Eng 2011;58(7):1950–8.

[57] Ikemoto S, DallaLibera F, Hosoda K. Noise-modulated neural networks as an application of stochastic resonance. Neurocomputing 2018;277:29–37.

[58] Ikemoto S. Noise-modulated neural networks for selectively functionalizing subnetworks by exploiting stochastic resonance. Neurocomputing 2021;448:1–9.

[59] Stocks NG. Suprathreshold stochastic resonance: an exact result for uniformly distributed signal and noise. Phys Lett A 2001;279:308–12.

[60] McDonnell MD, Stocks NG, Abbott D. Optimal stimulus and noise distributions for information transmission via suprathreshold stochastic resonance. Phys Rev E 2007;75(6):061105.

[61] Zhai Q, Wang Y. Optimal and suboptimal noises enhancing mutual information in threshold system. Fluct Noise Lett 2016;15(2):1650015.

[62] McDonnell MD, Stocks NG, Pearce CEM, Abbott D. Quantization in the presence of large amplitude threshold noise. Fluct Noise Lett 2005;5(3):L457–68.

[63] McDonnell MD, Gao X. M-ary suprathreshold stochastic resonance: Generalization and scaling beyond binary threshold nonlinearities. Europhys Lett 2014;108(6):60003.

[64] Cheng C, Zhou B, Gao X, McDonnell MD. M-ary suprathreshold stochastic resonance in multilevel threshold systems with signal-dependent noise. Physica A 2017;479:48–56.

[65] Zhou B, Wang X, Qi Q. Optimal weights decoding of M-ary suprathreshold stochastic resonance in stochastic pooling network. Chinese J Phys 2018;56(4):1718–26.

[66] Rousseau D, Duan F, Chapeau-Blondeau F. Suprathreshold stochastic resonance and noise-enhanced Fisher information in arrays of threshold devices. Phys Rev E 2003;68(3):031107.

[67] McDonnell MD, Abbott D, Pearce CEM. A characterization of suprathreshold stochastic resonance in an array of comparators by correlation coefficient. Fluct Noise Lett 2002;2(3):L205–20.

[68] Rousseau D, Chapeau-Blondeau F. Noise-improved Bayesian estimation with arrays of one-bit quantizers. IEEE Trans Instrum Meas 2007;56(6):2658–62.

[69] Patel A, Kosko B. Optimal mean-square noise benefits in quantizer-array linear estimation. IEEE Signal Process Lett 2010;17(12):1005–9.

[70] Li F, Duan F, Chapeau-Blondeau F, Abbott D. Signal estimation and filtering from quantized observations via adaptive stochastic resonance. Phys Rev E 2021;103(5):052108.

[71] McDonnell MD, Stocks NG, Pearce CEM, Abbott D. Optimal information transmission in nonlinear arrays through suprathreshold stochastic resonance. Phys Lett A 2006;352(3):183–9.

[72] Xu L, Vladusich T, Duan F, Gunn LJ, Abbott D, McDonnell MD. Decoding suprathreshold stochastic resonance with optimal weights. Phys Lett A 2015;379(38):2277–83.

[73] Xu L, Duan F, Abbott D, McDonnell MD. Optimal weighted suprathreshold stochastic resonance with multigroup saturating sensors. Physica A 2016;457:348–55.

[74] Chen H, Varshney PK, Michels JH. Noise enhanced parameter estimation. IEEE Trans Signal Process 2008;56(10):5074–81.

[75] Liu S, Yang T, Tang M, Wang P, Zhang X. Suitable or optimal noise benefits in signal detection. Chaos Solitons Fractals 2016;85:84–7.

[76] Liu J, Duan F, Chapeau-Blondeau F, Abbott D. Distributed Bayesian vector estimation using noise-optimized low-resolution sensor observations. Digit Signal Process 2021;118:103224.

[77] Zhai Q, Wang Y. Noise effect on signal quantization in an array of binary quantizers. Signal Process 2018;152:265–72.

[78] Widrow B. Statistical analysis of amplitude-quantized sampled-data systems. Trans Amer Inst Electr Eng Part II 1961;79(6):555–68.

[79] Schuchman L. Dither signals and their effect on quantization noise. IEEE Trans Commun Technol 1965;12(4):162–5.

[80] Gray RM, Stockham TG. Dithered quantizers. IEEE Trans Inform Theory 1993;39(3):805–12.

[81] Forbes C, Evans M, Hastings N, Peacock B. Statistical distributions. Fourth Edition.. Hoboken, New Jersey: John Wiley & Sons, Inc.; 2011.

[82] Luenberger DG. Optimization by vector space methods. New York: John Wiley & Sons, Inc.; 1969.